Modern Physics Letters B, Vol. 6, No. 20 (1992) 1217–1235

OPTICAL DIFFRACTIONS AS PROBES TO SURFACE DIFFUSION OF ADSORBATES

X. D. ZHU
Department of Physics, University of California, Davis, CA 95616-8677, USA

Received 27 July 1992

I review some of the general aspects of using optical diffractions from laser-induced surface density gratings to probe diffusion of adsorbates. Among examples, the recent progress in the study of quantum tunneling diffusions is emphasized.

1. Introduction

Diffusion of adsorbates on a surface is one of the fundamental steps in gas-solid interaction dynamics. A comprehensive understanding of surface diffusion is a prerequisite for understanding many surface dynamical processes such as catalytic reactions, epitaxial crystal growth, corrosion, and material processing.[1] Fundamentally, a moving particle on a surface is a sensitive probe to surface morphology. More recently, it has been demonstrated by Gomer and coworkers that the diffusion of light atoms on surfaces represents an important test case other than the diffusion of muons in solids for investigations of dissipative quantum tunneling.[2–7] The weaker surface potential modulation on a solid than its bulk counterpart leads to a larger delocalization of the wave functions of light adatoms and therefore an earlier onset of quantum tunneling diffusion.[8,9]

Despite of the strong research efforts both on the theoretical front and in the experimental area, the progress on the measurement of surface diffusion has been relatively slow. It is mainly limited by the nature of most existing techniques. A recent, extensive review has been given by Gomer.[1] As the measurement is often required to be performed on well-defined single crystal surfaces under ultrahigh vacuum condition, most usable techniques are limited either by difficult and unusual preparation procedures or by narrow dynamic ranges. Some suffer poor sensitivities and therefore are limited to high coverages. These difficulties have made the progress of a comprehensive, comparative study of surface diffusion over a large temperature range extremely slow. The latter is what is needed to appropriately address some of the current issues of diffusion such as quantum tunneling.[4–7,10–22]

Recently, we and a number of other groups have successfully explored optical diffractions from monolayer density gratings of adsorbates as probes to surface

diffusions.[23–28] The density gratings are created by laser-induced desorption with a pair of interfering laser pulses.[29–31] As the diffusive motion of remaining adsorbates tends to smear out the density modulation, the change of optical diffraction signals from the gratings is used to deduce surface diffusion coefficients. Both optical second-harmonic diffractions and linear optical diffractions have been explored and successfully employed to measure surface diffusion of a number of adsorbates.[23,24,26] This effort has been fueled by the most attractive features of an optical diffraction technique: (a) it can measure diffusion coefficients over 9 orders of magnitude, nominally from 10^{-7} cm^2/sec to 10^{-16} cm^2/sec. The low end is achieved by working with sub-micron density gratings; (b) it is readily employed to measure the anisotropy of a diffusion coefficient with an extremely high aspect ratio; (c) it has sensitivities to a few percent of one monolayer adsorbates; (d) adsorbate density grating preparation procedures using laser-induced thermal desorption and photo-desorption are readily compatible with conventional ultrahigh vacuum instrumentation, and are applicable to a large number of adsorbate-substrate systems; (e) the optical diffraction techniques are non-evasive to surface diffusion processes.

In this paper, I will briefly review some of the main experimental consideration and data analysis of this new technique. More experimental details can be found in the published literatures.[23–34] The key features of the optical diffraction techniques have been clearly illustrated in the few reported experiments.[23–28] As examples, I will describe briefly the experimental results of the diffusion of CO on Ni(111) and Ni(110), and hydrogen and deuterium on Ni(100). In the case of H and D on Ni(100), I show the evidence of a transition from an over-barrier diffusion to an activated tunneling diffusion.[26,28]

The organization of the paper is the following. In Sec. 2, the generation of monolayer gratings using laser-induced desorption is described. In Sec. 3, I present the theories of linear and nonlinear optical diffractions from these gratings. In Sec. 4, the evolution of the monolayer density grating under Fick's law and its detection are described. In Sec. 5, the application of the optical diffraction techniques in a number of surface diffusion measurements are briefly reviewed. Finally, I conclude by looking into possible directions of this research.

2. Generation of Monolayer Density Gratings by Laser-Induced Desorption With Interfering Optical Fields

Laser-induced gratings have long been exploited in studies of transient properties of material excitations including relaxation and transport in both gaseous and condensed media.[34] The laser-based techniques promise highest time-resolution ($< 10^{-13}$ sec) and highest spectral resolution for species selective excitation. The high aspect ratios of laser beam diameters to laser-induced grating spacings are ideal for studies of transport processes with anisotropy. It seems natural that laser-induced grating techniques should be applicable to surface transport measurements. For the purpose of a surface diffusion measurement, laser-induced gratings

present an appropriate length scale for the observation of the quantum tunneling effect.[2,3,26,28]

Applications of laser-induced dynamic gratings to studies of monolayer adsorbates, however, require extra experimental consideration.[29,32] This is because that linear optical diffraction intensities from gratings of one mono-atomic or monomolecular layer are at most 10^{-6} to 10^{-8} of incident beam intensities.[32] Therefore, the formation and the characterization of monolayer density gratings are experimentally much more challenging.

Generally, adsorbate density gratings can be produced through either resonant photo-desorption or thermal desorption effect. In the latter case, a substrate surface is heated in an interfering optical field of a laser pulse pair.[29–32] I will describe the thermal desorption method here.

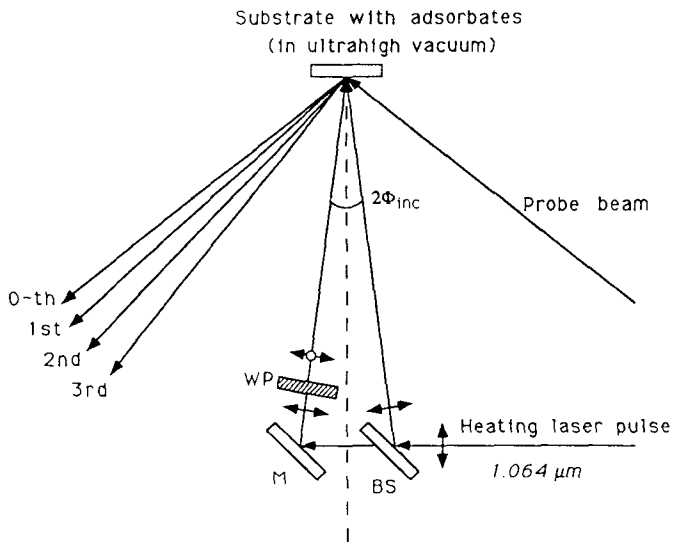

Fig. 1. Sketch of an experimental arrangement for the generation and detection of monolayer adsorbate density gratings with lasers. For surface diffusion measurements on single crystal substrates, the samples are placed in ultrahigh vacuum chambers. M is a dielectric mirror. BS is a beam splitter. WP is a half-wave plate which can change the linear polarization of the heating laser pulse from a *p*-wave (indicated by double arrows) to a *s*-wave (indicated by an open circle) continuously.

A typical experimental arrangement is shown in Fig. 1. A single crystal substrate is placed in an ultrahigh vacuum chamber. It exposes a low Miller index plane (e.g., [100], [110], and [111]) which is under investigation. The surface is usually cleaned through cycles of ion sputtering, annealing and oxidation *in vacuo*. The cleanliness is verified and characterized by Auger electron spectrometry. The substrate is then cooled to a measurement temperature at which adsorbates are allowed to cover the surface through gas phase deposition. By adjusting the dosage (in unit of Langmuir,

1 Langmuir = 10^{-6} torr-sec), the surface density or the coverage θ (defined as the ratio of the surface density to the saturation density) is controlled. The absolute coverage is determined by thermal desorption spectrometry and low energy electron diffraction measurement.[36]

For laser-induced thermal desorption, a Q-Switched Nd:YAG laser is used in our case.[23,26,29] It produces 10 ns optical pulses at wavelength $\lambda = 1.064\mu$m. The output pulse with an appropriate energy is split into two pulses with intensities I_1 and I_2, respectively. The two pulses are then brought to the sample surface at the incident angle Φ_{inc} but from two *different* sides of the surface normal (Fig. 1). This produces an intensity pattern at the sample surface with a periodicity

$$2a = \frac{\lambda}{2\sin\Phi_{inc}}. \tag{1}$$

The energy absorbed by the substrate heats up the surface region and thus creates a temperature grating.[29,37] The thermal desorption of the adsorbates by the temperature grating leads to a surface density grating. The desorption rate of adsorbates is usually described by[38]

$$\frac{d\theta}{dt} = -\nu\theta^n \exp\left(-\frac{E_{des}}{RT}\right). \tag{2}$$

ν is the pre-exponential factor, n is the desorption order, E_{des} is the desorption activation energy (in kcal/mol). They are known as the desorption kinetics parameters and are determined by extensive thermal desorption spectrometry measurements. R is the Boltzmann constant, and T is the temperature of the surface. As the desorption rate increases with the temperature rapidly, the desorption yield is significant only when the laser heating pulse is present.[39] Therefore, as long as grating spacings are small compared to thermal diffusion lengths (a fraction of micron for nanosecond heating laser pulses), the lateral heat conduction can be neglected so that the local surface density after desorption is determined only by the local optical intensity.[39] Knowing the kinetics parameters and the thermal constants of the substrate, the desorption yield and in turn the remaining adsorbate density can be determined to a high accuracy.[29,33] In practice, the calibration of the remaining surface density as a function of the heating laser intensity or fluence (J/cm^2) can be easily obtained experimentally using, for example, an optical second-harmonic generation micro-probe to monitor the adsorbate density.[33] From the calibration, one can choose I_1 and I_2 to produce a prescribed surface density grating. In Fig. 2, I show an example of a calibration of the coverage change $\Delta\theta$ versus the absorbed fluence for CO on Ni(111).[29]

Experimentally, I_1 and I_2 is usually set by a properly chosen beam splitter. In practice, it is more desirable to use a nominal 50–50 beam splitter and use a polarization rotation device (e.g., a half-wave plate) on one arm so that the polarization of the arm can be set continuously from being orthogonal to being

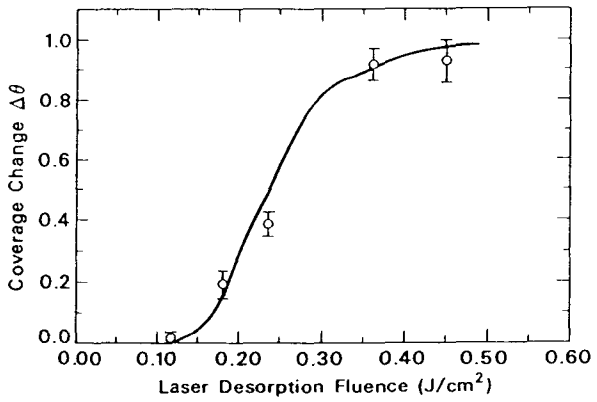

Fig. 2. The coverage change of CO on Ni(111) $\Delta\theta$ versus the absorbed laser fluence in a laser-induced thermal desorption measurement. $\Delta\theta$ is deduced from the change of a calibrated, *in-situ* optical second-harmonic generation. The solid line is calculated from the desorption kinetics parameters.[33,39]

parallel to that of the other arm. If the angle of polarization rotation from the parallel position is α, the intensity of the interfering optical field at the sample surface is given by

$$I(x) = I_1 + I_2 + 2\sqrt{I_1 I_2}\cos\alpha\cos[4\pi\sin\Phi_{\text{inc}}x/\lambda]\,. \tag{3}$$

In this way, we can choose the sum of I_1 and I_2 to yield a prescribed average coverage θ_0, and the polarization angle α to produce a desired modulation depth $\Delta\theta$.

From the symmetries of the intensity distribution and in turn the laser-induced adsorbate density $\theta(x,t)$, one can always expand $\theta(x,t)$ in the following spatial Fourier series,[39]

$$\begin{aligned}\theta(x,t) &= \sum_{n=0}\theta_n(t)\cos(n\pi x/a)\\ &= \sum_{n=0}\frac{\theta_n(t)}{2}\left[\exp(in\pi x/a)+\exp(-in\pi x/a)\right].\end{aligned} \tag{4}$$

The time dependence comes from the diffusion of adsorbates at finite temperatures.[1] At low enough temperatures, one can characterize the grating with optical diffractions before the effect of the diffusion sets in Refs. 29–32. In Fig. 3, I show a calculated grating profile of CO on Ni(111) near the center of a laser pulse pair based upon the calibration curve in Fig. 2. The profile was confirmed by the optical second-harmonic diffraction measurement which is described next.[29]

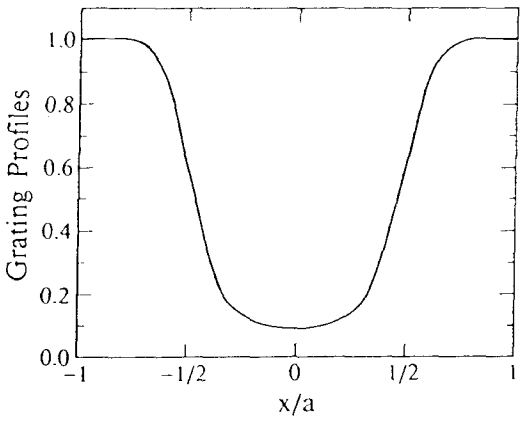

Fig. 3. A calculated grating profile of a monolayer grating of CO on Ni(111) within one spatial period $2a$ using the calibration shown in Fig. 2.[29]

3. Detection of a Monolayer Adsorbate Density Grating by Optical Diffractions

The general consideration of linear and nonlinear optical diffractions from a monolayer adsorbate density grating is very similar.[31,32,40–42] When a probe laser beam with an electric field $\mathbf{E}_{\text{inc}}(\omega)\exp[i(\mathbf{k}_1\mathbf{r}-\omega t)]$ is incident on a substrate covered with adsorbates, the linear and second-order nonlinear optical responses of the surface layer can be characterized by a dipole sheet oscillating at $\omega, \mathbf{P}_s(\omega) = \chi^{(1)}(\omega)\mathbf{E}_{\text{inc}}(\omega)$ and a dipole sheet oscillating at $2\omega, \mathbf{P}_s(2\omega) = \chi^{(2)}(2\omega)\mathbf{E}_{\text{inc}}(\omega)\mathbf{E}_{\text{inc}}(\omega)$, respectively. When the adsorbate density is modulated as expressed by Eq. (5), the linear and the nonlinear dipolar responses are also modulated. If the effect of adsorbate-adsorbate interactions is negligible or when the modulation of the density is small, we expect both $\mathbf{P}_s(\omega)$ and $\mathbf{P}_s(2\omega)$ to be directly proportional to the surface density $\theta(x,t)$,[31,32]

$$\mathbf{P}_s(\omega) = \mathbf{P}_{s,0}(\omega)\theta(x,t)\,, \tag{5}$$

$$\mathbf{P}_s(2\omega) = \mathbf{P}_{s,0}(2\omega)\theta(x,t)\,. \tag{6}$$

The radiation at either ω or 2ω from an oscillating dipole sheet can be obtained by solving Maxwell equations or directly summing up the radiation from all the oscillating dipoles.[40] For a modulated dipole sheet, one calculates the radiation corresponding to each spatial Fourier component of Eq. (5) or Eq. (6) separately.[31,32] For example, the nth order diffraction in reflection is given by[32]

$$E_{p,n} = \frac{i2\pi k_1}{\varepsilon_1 k_{1z}}\left[k_{1z}L_{xx}P_{s,0x} + k_{1x}L_{zz}P_{s,0z}\right]\frac{\theta_n(t)}{2}\,, \tag{7}$$

$$E_{s,n} = \frac{i2\pi k_1^2}{\varepsilon_1 k_{1z}}L_{yy}P_{s,0y}\,\frac{\theta_n(t)}{2}\,. \tag{8}$$

Here L_{xx}, L_{yy}, and L_{zz} are the macroscopic local field factors due to the difference of dielectric constants of the monolayer ε', the incidence medium ε_1, and the transmission medium ε_2.[40] k_1 is the magnitude of the wave vector $\mathbf{k}_1$ in medium ε_1, k_{1x} and k_{1z} are components of $\mathbf{k}_1$. The output signal in reflection in photon per second is given by[40]

$$S_{p(s),n}(\omega) = \frac{c\sqrt{\varepsilon_1}}{2\pi} |E_{p(s),n}(\omega)|^2 \frac{Af\tau}{\hbar\omega}. \tag{9}$$

Here A is the area of the dipole sheet normal to the diffraction direction. f is the repetition rate of a probe laser, and τ is its pulsewidth. For a continuous wave laser, $f\tau$ is taken as unity.

The direction of the nth order diffraction is determined by the usual requirement on the tangential component $k_{n,x}$ of the diffracted radiation wave vector $\mathbf{k}_n$,

$$k_{n,x}(\omega) = k_{1x}(\omega) \pm \frac{n\pi}{a}, \tag{10}$$

for linear optical diffractions, and

$$k_{n,x}(2\omega) = 2k_{1x}(\omega) \pm \frac{n\pi}{a}, \tag{11}$$

for optical second-harmonic diffractions.

We now estimate typical signal strengths for both linear and second-harmonic diffractions. For linear optical diffractions, the signal strengths without local field factor correction can be expressed approximately as

$$S_{p(s),n}(\omega) = S_{\text{inc}}(\omega) \frac{64\pi^4}{\lambda^2} |N_s \alpha^{(1)}(\omega)|^2 \left(\frac{\theta_n}{2}\right)^2. \tag{12}$$

For $N_s\alpha^{(1)}(\omega) \sim 5 \times 10^{-9}$ esu, $\theta_n \sim 0.4$, $\lambda \sim 5 \times 10^{-5}$ cm,

$$S_{p(s),n}(\omega) \sim 2 \times 10^{-6} S_{\text{inc}}(\omega). \tag{13}$$

Including the local field factor may reduce the signal strengths into 10^{-7} range. For optical second-harmonic diffractions, the signal strengths without local field factor correction are given similarly by

$$S_{p(s),n}(2\omega) = S_{\text{inc}}(\omega) \frac{64\pi^4}{\lambda^2} |N_s \alpha^{(2)}(2\omega) E_{\text{inc}}(\omega)|^2 \left(\frac{\theta_n}{2}\right)^2. \tag{14}$$

For a 10 ns laser pulse, a typical peak intensity limited by optical damages for metal substrates is 10 MW/cm^2. This corresponds to $E_{\text{inc}}(\omega) \sim 10^2$ esu. For $N_s\alpha^{(2)}(2\omega) \sim 10^{-15}$ esu, we have $N_s\alpha^{(2)}(2\omega)E_{\text{inc}}(\omega) \sim 10^{-13}$ esu.[40] Thus for $\theta_n \sim 0.4$, $\lambda \sim 5 \times 10^{-5}$ cm,

$$S_{p(s),n}(2\omega) \sim 10^{-15} S_{\text{inc}}(\omega). \tag{15}$$

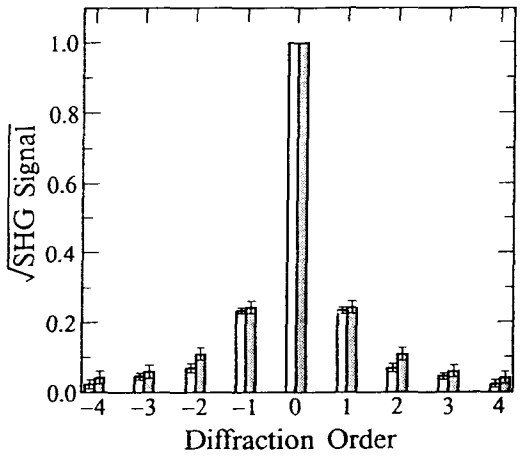

Fig. 4. The square roots of optical second-harmonic diffractions $[S_n(2\omega)]^{1/2}$ [see Eq. (14) in the text] vs the diffraction order from a monolayer grating of CO on Ni(111) as shown in Fig. 3 (Ref. 29). Unshaded columns: measured signals. Shaded columns: calculated signals from the results of Fig. 3.

In Fig. 4, I show the optical second-harmonic diffractions versus the diffraction order from a grating of a monolayer CO on Ni(111) as depicted in Fig. 3.[29] The shaded columns are calculated from the curve shown in Fig. 3. The agreement is very well. In Fig. 5, I show the linear optical diffractions of a He-Ne laser up to 5th order from a grating of a monolayer Rh6G molecules on fused silica. It should be noted that in this case, the linear diffractions are not resonance-enhanced at the He-Ne laser wavelength and therefore represents a typical case of what one should expect.[32]

From Eq. (13) and Eq. (15), it is clear that the strengths of linear optical diffractions are 10^8 times of optical second-harmonic diffractions for same averaged probe beam powers. It is thus necessary to comment on the usefulness of nonlinear optical diffractions. It is known that linear optical diffractions are accompanied by a diffuse scattering background from the residual roughness on a nominally flat substrate.[32] The unwanted background is the regular bulk reflection from optically rough regions. As a linear bulk reflection is 10^6 times as intense as that from a monolayer, an optically rough region of 10^{-6} of the total illuminated surface area is sufficient to yield a background light which overwhelms linear optical diffractions from monolayer gratings. Special cares thus must be taken to eliminate the background contribution.

This problem is lifted by symmetry in optical second-harmonic diffractions.[29] Although being a much weaker optical process, the diffuse scattering from the bulk at the second-harmonic frequency is dramatically suppressed when substrates have centers of inversion or an isotropic order.[40,43,44] The residual diffuse second-

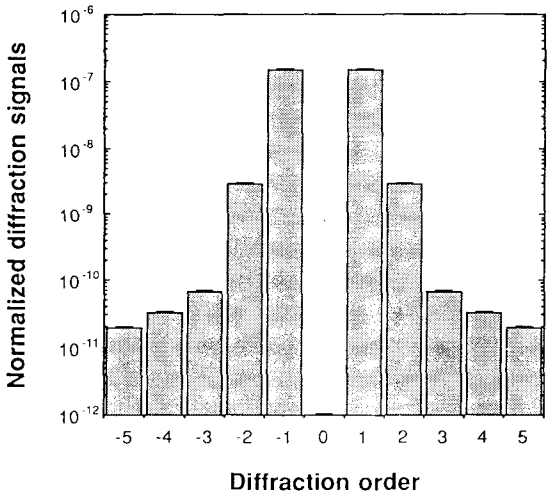

Fig. 5. The measured linear optical diffraction signals vs. the diffraction order [see Eq. (12) in the text]. All signals are normalized to the strength of an incident He-Ne laser beam.[32]

harmonic scattering comes mainly from much weaker electric quadrupole and magnetic dipole responses of the bulk.[45] Consequently, the ratio of second-harmonic diffractions from monolayer adsorbate gratings to the diffuse second-harmonic background is enhanced by a factor of 10^4 to 10^6 from that of a linear optical diffraction. This has enabled Reider *et al.*, Zhu *et al.*, and Suzuki *et al.* to observe the optical second-harmonic diffractions from monolayer adsorbate gratings to high orders.[29–31]

The only disadvantage of optical second-harmonic diffractions is the weakness of its absolute strength.[40] Limited by optical damages, first-order optical second-harmonic diffractions from a fully modulated monolayer adsorbate density grating with an area of 10 mm^2 are typically 0.05–0.2 photon-counts per laser pulse.[23,25] For modulations less than 10% of one monolayer, diffraction signals decrease quickly to a prohibitively low level. This makes a coverage dependence investigation very difficult.

This difficulty with the nonlinear probe has led us to revisit the linear diffraction technique. Recently, by effectively suppressing the diffuse scattering background with spatial filtering techniques, we successfully demonstrated the feasibility of using linear optical diffractions to probe monolayer adsorbate density gratings.[32] More recently, Xiao *et al.* also successfully explored the detection of linear optical diffractions by using a polarization modulation technique.[46]

Generally speaking, for substrate systems which exhibit large changes in surface nonlinear optical responses upon adsorption of adsorbates such as hydrogen on Si(111) and CO on Ni(111), optical second-harmonic diffractions can be justified as good choices as probes to surface density gratings. In these cases, the signal strengths are no longer a drawback to the advantage of automatically low diffuse scattering background. Otherwise, linear optical diffractions are better choices.

4. Evolution of a Monolayer Adsorbate Density Grating and the Measurement of Surface Diffusion Coefficients

At a finite temperature T, an adsorbate density grating evolves in time according to the Fick's law. Since the overall size of a laser-induced grating (a few millimeters) is much larger than the grating periodicity (a few microns), we have at hand a one-dimensional diffusion problem,

$$\frac{\partial\theta}{\partial t} = \frac{\partial}{\partial x}\left[D(\theta)\frac{\partial\theta}{\partial x}\right]. \tag{16}$$

The one dimensionality is characterized by aspect ratios of 10^3 to 10^4. $D(\theta)$ is the chemical diffusion coefficient which includes the effect of adsorbate-adsorbate interactions after an appropriate thermodynamic average.[1] It is to be distinguished from a tracer diffusion coefficient which is obtained at the zero coverage. When the interaction is of short range and thus acts only to block the available destiny sites for a moving adsorbate or when the measurement is performed at low coverages, the chemical diffusion coefficient is expected to approach the tracer diffusion coefficient. Such an approximation is useful as most microscopic theories of diffusion coefficients are established in the zero coverage limit.

When the coverage dependence of the diffusion coefficient $D(\theta)$ is weak for a given coverage modulation $\Delta\theta$, we can approximate Eq. (16) by replacing $D(\theta)$ with $D(\theta_0)$. The nth spatial Fourier component of the adsorbate density grating $\theta_n(t)$ [Eq. (4)] is then easily obtained,

$$\theta_n(t) = \theta_n(0)\exp[-n^2\pi^2 D(\theta_0)t/a^2]. \tag{17}$$

From Sec. 2, we find that optical diffraction signals versus t are given as

$$S_n(t) = S_n(0)\exp[-2\pi^2 n^2 D(\theta_0)t/a^2]. \tag{18}$$

By measuring the time-dependent diffraction signals, one extracts $D(\theta_0)$ from the exponents. It should be noted here that higher order Fourier components decay much faster than the lower order ones. This may be exploited to further enhance the dynamic range of optical diffraction techniques.

I now comment on the dynamic range offered by optical diffraction techniques and its usefulness. I should first note that a diffusion coefficient $D(\theta_0)$ is a complex function of adsorbate-adsorbate and adsorbate-substrate interactions. The investigation of the latter forms the central issues of surface diffusion research.[1,10–22] Often, the physical mechanisms which govern the diffusion or the transport of an adsorbate along the surface are clearly distinguished and characterized only by measuring surface diffusion coefficients over a large parameter space including temperature, surface densities, isotope masses, length scales of the diffusion, and surface morphologies.[1] Optical diffraction techniques offer a large dynamic range to meet

such a demand. From Eq. (13), we see that the range of measurable diffusion coefficients is nominally determined by

$$D \sim \frac{a^2}{2\pi^2 n^2 t}. \tag{19}$$

Typically, $t \sim 10$ to 10^4 sec which is determined by signal-to-noise ratios and contaminations due to adsorption of ambient gases in a 10^{-10} to 10^{-11} torr vacuum. With $a \sim 10^{-2}$ to 10^{-5} cm, we arrive at an estimate of the range of measurable D from 5×10^{-7} cm^2/sec to 5×10^{-16} cm^2/sec, if the first order diffraction is measured. The lower limit may be extended further when higher order diffractions are employed. Very few techniques can match the performance of dynamics range of the optical diffraction techniques.[1] It has made it possible for us to study the quantum tunneling diffusion which only sets in at low temperatures with D in the range below 10^{-10} cm^2/sec.[2,3,5,26] As shown in the examples in the next section, the wide applicability of optical diffraction techniques has opened up many possibilities in the fields of surface diffusion research and the studies of massive particle transport in solid in general.

5. Application of Optical Diffractions in the Studies of Surface Diffusion of Adsorbates

There have been numerous reports of surface diffusion measurements by using optical diffractions from surface density gratings. Early works by Maiya, Blakely, Bonzel, and Yamashita *et al.* on self-diffusion and the anisotropy of surface energy by using linear diffractions involved photolytically etched periodic profiles on surfaces of single crystal metals.[47–50] These profiles are tens of microns wide and a fraction of a micron deep. In these studies, steps of high densities and facets are involved in the surface diffusion processes and therefore may affect the diffusion measurement directly and also indirectly through altering the properties of neighboring low Miller index terraces. Recently, Zhu *et al.* [CO on Ni(111)] and Reider *et al.* [H on Si(111)] successfully performed the measurements of surface diffusion coefficients by using optical second-harmonic diffractions.[23,24] Later, Xiao *et al.* applied the optical second-harmonic diffractions to the measurement of anisotropic diffusion of CO on Ni(110).[25,27] More recently, we applied linear optical diffractions to the studies of hydrogen and deuterium on Ni(100) down to 120 K and observed what we believe the onset of an activated tunneling motion.[26,28]

5.1. *Measurements of slow over-barrier diffusions: CO on Ni(111) and H on Si(111)*

In a macroscopic diffusion measurement, one usually observes the evolution of a preformed particle density profile with an appropriate probe. The length scale L of the macroscopic diffusion is determined by either the method of the density profile formation or by the probe. This sets a lower limit of measurable diffusion coefficient

D_{min} for a given technique if there exists an upper limit on the measurement time t_{max} in the experimental requirement,

$$D_{min} \sim \frac{L^2}{t_{max}}. \tag{20}$$

The proportionality constant is typically 0.1 [see Eq. (19)]. For a measurement of diffusion of adsorbates on a well-defined single crystal, t_{max} is the time beyond which the re-adsorption from an ambient of an ultrahigh vacuum chamber becomes unacceptable. For an operating base pressure of 1×10^{-10} torr, t_{max} is nominally 10^4 sec which is the time for a dosage of one Langmuir.[36] If we assume that all the gaseous species which strike the surface during t_{max} remain on the surface, a dosage of one Langmuir will cover a clean surface with roughly a full monolayer of "impurity adsorbates".

In a temperature range when over-barrier diffusions dominate, it is sometimes possible to raise the surface temperature to lift the diffusion rate over D_{min}. However, this has been shown to be limited by the thermal desorption.[23,24] D_{min} is thus an important characteristics of an experimental probe. For a Field emission microscope used by Gomer and coworkers, the length scale L is about 500 Å and is determined by the metal emission tip. The minimum measurable diffusion coefficient is nominally $D_{min} \sim 2 \times 10^{-16}$ cm^2/sec according to Eq. (20). For the laser-induced hole-burning mass spectrometry technique of George *et al.*, the length scale is limited by the spot size of a heat laser beam to 300 μm (Refs. 51 and 52) so that $D_{min} \sim 1 \times 10^{-9}$ cm^2/sec. As demonstrated in the following experiments, the capability of detecting small diffusion coefficients or better still having a large dynamic range from 10^{-7} to 10^{-16} cm^2/sec [see the previous Section] is one of the most useful virtues of the optical diffraction technique.

The study of CO on Ni(111) is the first case of using optical diffractions from laser-induced monolayer density gratings in a surface diffusion measurement.[23] It was after a failed attempt to measure the diffusion with a laser-induced coverage "hole-burning" and refilling technique.[51] By depleting the pre-adsorbed CO over a 1 mm^2 area centered on a larger Ni(111) surface with one heating laser pulse and monitoring the refilling of CO from the surrounding region with an *in-situ* optical second-harmonic generation probe, Zhu *et al.* observed no sign of diffusion for a time of 5 hours at temperatures just low enough to avoid a substantial thermal desorption. This prompted the development of the optical second-harmonic diffraction probes by Zhu *et al.* so that the diffusion of CO on Ni(111) could be examined at a much smaller length scale.[23]

In Fig. 6, I reproduce the first order optical second-harmonic diffractions from monolayer gratings of CO on Ni(111) versus the observation time. The measurements were carried out from 220 K to 270 K. The grating spacing $2a$ was chosen to be 20 μm. The decay of the diffraction signal is fit to a single exponential function. The diffusion coefficients $D(T)$ are obtained from the exponents using Eq. (18). To display the temperature dependence, $D(T)$ is plotted in the Arrehnius form in Fig. 7.

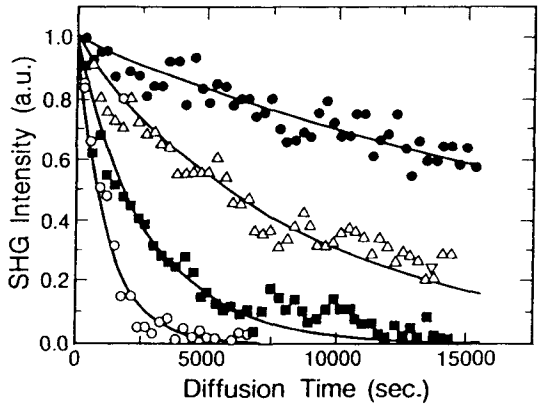

Fig. 6. Normalized first-order optical second-harmonic diffraction signals from monolayer gratings of CO on Ni(111) vs. the observation time. Solid circles: $T = 219$ K; open triangles: $T = 247$ K; solid squares: $T = 261$ K; open circles: $T = 273$ K. The solid curves are least-square fits using single exponential functions [see Eq. (18)].

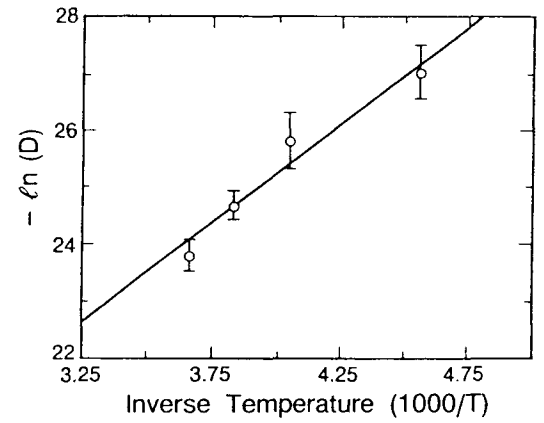

Fig. 7. Arrehnius plot (open circles) of the diffusion coefficients $D(T)$ of CO on Ni(111) from 219 K to 273 K obtained from the results shown in Fig. 6.

Within the error of the measurement, it is fit reasonably well with a functional form of $D(T) = D_0 \exp(-E_{\text{diff}}/RT)$. From the fit, the diffusion activation energy E_{diff} is determined as 7 kcal/mol, and the diffusivity $D_0 = 1.2 \times 10^{-5}$ cm^2/sec.[23] It was attributed to an over-barrier diffusion. From an energetics analysis, it was tentatively suggested that CO is likely to move along the route from a bridge site over a terminal site (on-top site) and to a neighboring bridge site.[39] It is interesting to note that if the grating spacing was instead taken to be 1 mm, the diffusion would be noticeable only at 700 K over 10000 seconds. By then the adsorbed CO would

have been long gone. This explains the earlier failure to measure the diffusion of CO on Ni(111) with the laser-induced hole burning and refilling technique.

Another example of slow diffusion is that of strongly chemisorbed hydrogen on Si(111).[24] It was recently investigated by Reider *et al.* with the optical second-harmonic diffractions from laser-induced hydrogen density gratings. The authors had to use grating spacings of one quarter of a micron in order to curtail the thermal desorption effect to a manageable level.

5.2. *Study of anisotropy of surface diffusion: CO on Ni(110)*

One of the strong features of optical diffractions is the capability to resolve the anisotropy of a surface diffusion with an extremely high aspect ratio, nominally 10^3 to 10^4.[25,27,39] Xiao, Zhu, Daum and Shen studied the anisotropy of the diffusion of CO on Ni(110).[25,27] By rotating the grating with respect to a surface crystalline axis, e.g., [100] axis, the diffusion coefficient versus the azimuthal angle ψ was determined. The diffusion coefficient $D(T)$ is reproduced in Fig. 8. From the results, the authors were able to identify two distinct diffusion channels, one along [110] direction with $E_{\text{diff}} = 1.1$ kcal/mol and $D_0 = 3.8 \times 10^{-9}$ cm^2/sec and the other along [100] with $E_{\text{diff}} = 3.1$ kcal/mol and $D_0 = 4.8 \times 10^{-6}$ cm^2/sec. This is experimentally significant since there does not exist *a priori* knowledge on what the surface potential distribution is or should be like for CO on Ni(110) or on any other surfaces. It is noted that the activation energy along [110] axis, $\sim$ 1 kcal/mol, is rather small. It is thus conceivable that adsorbate-adsorbate interactions and the presence of impurities can easily lift the preference of specific sites on the ridges of [110] Ni atom rows. This is consistent with the reports of rich superlattice structures of overlayer CO at different coverages, particularly the molecular arrangements along [110] rows. The details of the experiment and the analysis can be found elsewhere.[25,27]

Unlike CO on Ni(111) and H on Si(111), optical second-harmonic diffractions from monolayer gratings of CO on Ni(110) represent a case of weak signals. Due to a much smaller change of the nonlinear susceptibility of a Ni(110) surface upon adsorption of CO, the first order diffraction signal was only 0.05 photon counts per pulse.[25] With a fully modulated CO grating, in order to obtain a signal-to-noise ratio of 10, each data point takes at least 4 minutes when using a probe laser with a repetition rate of 10 Hz. For modulations much less than 50% of a monolayer, diffraction signals quickly drop to a prohibitively low level. This demonstrates the difficulty of applying optical second-harmonic diffractions to coverage dependence studies when a much smaller surface density modulation $\Delta\theta$ is required.

5.3. *Study of quantum tunneling diffusions: H and D on Ni(100)*

The diffusion of light atoms in solids through quantum tunneling mechanisms is one of the most actively studied topics in condensed matters physics.[2–4,7,10–22] There have been intensive effort in the research of dissipative tunneling under the influ-

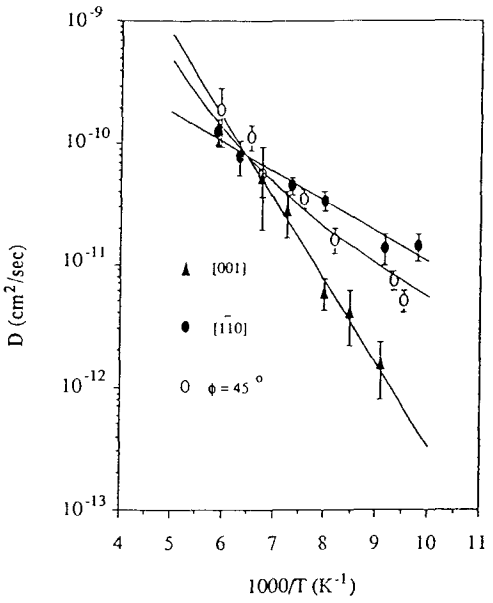

Fig. 8. Arrehnius plots of the diffusion coefficients $D(T, \psi)$ for CO on Ni(110). ψ is the azimuthal angle between the [110] axis of the Ni substrate and the orientation of the CO coverage grating. Solid triangles: $\psi = 0°$, i.e., macroscopic diffusion along [001] axis. Solid circles: $\psi = 90°$, i.e., macroscopic diffusion along [11] axis. Open circles: $\psi = 45°$.

ences of phonons, conduction electrons, and other low lying excitations in solids. Hydrogen isotopes on metals and semiconductors are ideal candidates for a thorough experimental exploration.[2,3,26,28] The diffusion due to the quantum tunneling effect becomes dominant at fairly low temperatures and is typically in the range of 10^{-10} to 10^{-14} cm^2/sec.[2-5,7] Optical diffraction probes are among the very few techniques which are capable of measuring such a slow diffusion. In addition, with the improved sensitivity of linear diffraction probes, the measurements can be extended to a large number of substrate systems and large ranges of coverages. This makes comparative and comprehensive investigations possible.

It is in this spirit that we started the present investigation of the diffusion of hydrogen isotopes on metals using a linear optical diffraction method.[26,28] We have measured diffusion coefficients for hydrogen and deuterium on Ni(100) in the temperature range from 200 K to 120 K. In these measurements, the grating half-period a of 8.3 μm and 4.2 μm has been used, partly to check the consistency. The average coverages θ_0 in both cases are 0.7. The modulation of the gratings is less than 10% of one monolayer. Thus, we can apply Eq. (18) to the analysis. The first order diffraction of a 2 mW He-Ne laser is used to probe the evolution of the hydrogen coverage gratings.[26,32] The measured $D(T)$ for hydrogen and deuterium are plotted in Fig. 9 and Fig. 10, respectively. The results clearly indicate that the diffusion of both isotopes in the investigated temperature range is characterized by two thermally

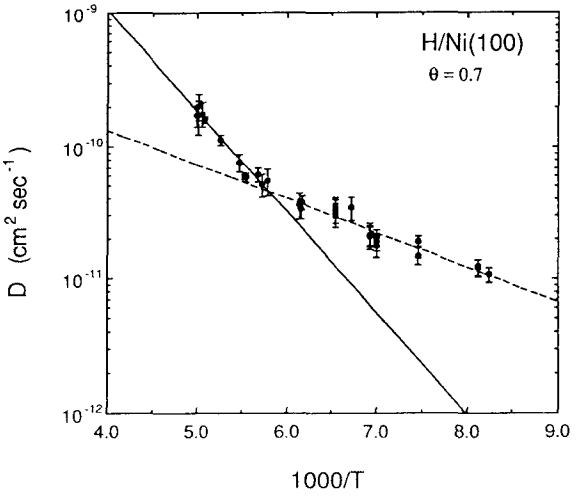

Fig. 9. Arrehnius plot of the diffusion coefficient $D(T)$ for hydrogen atoms on Ni(100) at a coverage $\theta = 0.7$. The temperature range is from 120 K to 200 K. The kink in the data occurs at $T = 160$ K. Solid line: an Arrehnius fit to the high temperature behavior. Dash line: an Arrehnius fit to the low temperature behavior.

activated processes. From the fits to Arrehnius forms $D(T) = D_0 \exp(-E_{\text{diff}}/RT)$, we have deduced the diffusivities D_0 and the activation energies E_{diff}. For hydrogen, $D_0 = 1.1 \times 10^{-6}$ cm^2/sec, and $E_{\text{diff}} = 3.5$ kcal/mol from 200 K to 160 K, and $D_0 = 1.5 \times 10^{-9}$ cm^2/sec, and $E_{\text{diff}} = 1.2$ kcal/mol from 160 K to 120 K. For deuterium, $D_0 = 5 \times 10^{-5}$ cm^2/sec, and $E_{\text{diff}} = 5.0$ kcal/mol from 200 K to 170 K, and $D_0 = 9 \times 10^{-10}$ cm^2/sec, and $E_{\text{diff}} = 1.05$ kcal/mol from 170 K to 120 K. Our results at high temperatures confirm the earlier measurements at even higher temperatures by other groups using the field emission microscope and laser-induced hole-burning mass spectrometry techniques.[3,51,52] It is attributed to be an over-barrier hopping from a four-fold hollow site over a two-fold bridge site to a neighboring hollow site. We presently attribute the low temperature activated diffusion to an activated tunneling as described by the small-polaron model due to Holstein.[10] As has been analyzed in detail in Ref. 28, the experimentally measured activation energy, 1 kcal/mol, correlates well with an estimate of the lattice relaxation energy based upon the available surface phonon data on Ni(100).[53–57]

We should point out that the issue is far from settled as we observed little isotope mass dependence of the tunneling matrix elements J which are deduced from the measured diffusivities.[7,10] It presents a difficulty to reconcile with conventional small-polaron theories.[7,10] We are extending the measurement to much lower temperatures ($\sim$ 20 K) in order to fully investigate the temperature dependence of $D(T)$ and in turn the roles of different low energy excitations of metals in the tunneling of hydrogen isotopes.

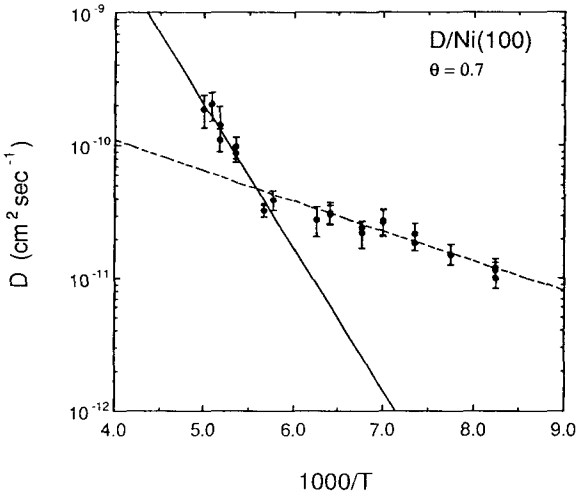

Fig. 10. Arrehnius plot of the diffusion coefficient $D(T)$ for deuterium atoms on Ni(100) at a coverage $\theta = 0.7$. The temperature range is from 120 K to 200 K. The kink in the data occurs at $T = 170$ K. Solid line: an Arrehnius fit to the high temperature behavior. Dash line: an Arrehnius fit to the low temperature behavior.

6. Concluding Remarks

Optical diffractions from surface density gratings as probes to diffusion of adsorbates are very promising. In the few reported experiments, their most desirable features are shown to be ideally suited for the purpose. We are at the stage when in-depth investigations are possible and practical. We have just started a long-term research on the experimental aspects of quantum tunneling diffusions of light atoms. The goal is to elucidate the mechanisms behind the dissipative tunneling and the roles of such parameters as phonons, conduction electrons, surface morphology, adsorbate-adsorbate and adsorbate-substrate interactions. In addition, we will see more experimental data obtained by optical diffraction probes over much larger ranges of temperature and other static and kinetic parameters such as coverages, coadsorption, and vicinal surfaces. This will surely improve and further our current understanding of surface diffusion in a more complete and coherent fashion.

Acknowledgements

The author wishes to sincerely thank Professor Y.R. Shen, Th. Rasing, W. Daum, Xudong Xiao, A. Lee, A. Wong, and U. Linke for the collaboration at various stages of the development of the optical diffraction technique. This work has been supported by the Director, Office of Energy Research, Office of Basic Energy Sciences, Materials Sciences Division of the U.S. Department of Energy under Contract No.

DE-AC03-76SF00098, by the National Science Foundation under Grant No. DMR-9104109 and in part by American Chemical Society under the Petroleum Research Fund No. 24373G5.

References

1. Gomer, *Rep. Prog. Phys.* **53**, 917 (1990).
2. R. DiFoggio and R. Gomer, *Phys. Rev.* **B25**, 3490 (1982); S. C. Wang and R. Gomer, *J. Chem. Phys.* **83**, 4193 (1985); C. Dharmadhikari and R. Gomer, *Surf. Sci.* **143**, 223 (1984); E. A. Daniels, J. C. Lin, and R. Gomer, *Surf. Sci.* **204**, 129 (1988); A. Auerbach, K. F. Freed, and R. Gomer, *J. Chem. Phys.* **86**, 2356 (1987).
3. T.-S. Lin and R. Gomer, *Surf. Sci.* **225**, 41 (1991).
4. K. W. Fehr, in *Hydrogen in Metals I*, ed. G. Alefeld and J. Völkl (Springer, 1978), Chap. 8, pp. 197–226; J. Völkl and G. Alefeld, *ibid.*, Chap. 12, pp. 321–348.
5. G. Grebennik, I. I. Gurevich, V. A. Zukov, I. G. Ivanter, A. P. Manych, B. A. Nikol'skii, V. I. Selivanov, V. A. Suetin, *Sov. Phys.- JETP* **41**, 777 (1976).
6. H. Teichler, *Phys. Lett.* **64A**, 78 (1977).
7. R. K. Kiefl, R. Kadono, J. H. Brewer, G. M. Luke, H. K. Yen, M. Celio, and E. J. Ansaldo, *Phys. Rev. Lett.* **62**, 792 (1989).
8. M. J. Puska, R. M. Nieminen, M. Manninen, B. Chakraborty, S. Holloway, and J. K. Norskov, *Phys. Rev. Lett.* **51**, 1081 (1983), and references therein.
9. M. J. Puska and R. M. Nieminen, *Surf. Sci.* **157**, 413 (1985).
10. T. Holstein, *Ann. Phys.* **8**, 343 (1959).
11. C. P. Flynn and A. M. Stoneham, *Phys. Rev.* **B1**, 3966 (1970).
12. J. Kondo, *Physica* **84B**, 40 (1976); *ibid.* **126B**, 377 (1984); *ibid.* **125B**, 279 (1984); *ibid.* **141B**, 305 (1986).
13. A. J. Leggett, S. Chakravarty, A. T. Dorsey, M. P. A. Fisher, A. Garg, and W. Zwerger, *Rev. Mod. Phys.* **59**, 1 (1987).
14. J. P. Sethna, *Phys. Rev.* **B24**, 698 (1981); *ibid* **25**, 5050 (1982).
15. U. Weiss and M. Wollensak, *Phys. Rev. Lett.* **62**, 1663 (1989).
16. H. Grabert and U. Weiss, *Phys. Rev. Lett.* **54**, 1605 (1985).
17. M. P. A. Fisher and A. T. Dorsey, *Phys. Rev. Lett.* **54**, 1609 (1985).
18. M. I. Klinger, *Phys. Rep.* **94**, 183 (1983).
19. V. I. Gol'danskii, L. I. Trakhtengerg, and V. N. Fleurov, *Tunneling phenomena in Chemical Physics*, English translated by V. N. Fleurov (Gordon and Breach, 1989), Chap. 7, pp. 223–242.
20. Q. Niu, *J. Stat. Mech.* **65**, 317 (1991), and references therein.
21. K. B. Whaley, A. Nitzan, and R. B. Gerber, *J. Chem. Phys.* **84**, 5181 (1986); P. D. Reilly, R. A. Harris,and K. B. Whaley, *J. Chem. Phys.* **95**, 8599 (1991).
22. K. A. Muttalib and J. P. Sethna, *Phys. Rev.* **B32**, 3462 (1985).
23. X. D. Zhu, Th. Rasing, and Y. R. Shen, *Phys. Rev. Lett.* **61**, 2883 (1988).
24. G. A. Reider, U. Hofer, and T. F. Heinz, *Phys. Rev. Lett.* **66**, 1994 (1991).
25. Xudong Xiao, X. D. Zhu, W. Daum, and Y. R. Shen, *Phys. Rev. Lett.* **66**, 2352 (1991).
26. X. D. Zhu, A. Lee, A. Wong, and U. Linke, *Phys. Rev. Lett.* **68**, 1862 (1992).
27. Xudong Xiao, X. D. Zhu, W. Daum, and Y. R. Shen, *Phys. Rev.* **B**, (in press, 1992).
28. A. Lee, X. D. Zhu, L. Deng, and U. Linke, submitted to *Phys. Rev.* **B**.
29. X. D. Zhu and Y. R. Shen, *Opt. Lett.* **14**, 503 (1989).
30. G. A. Reider, M. Huemer, and A. J. Schmidt, *Opt. Commun.* **68**, 149 (1988).
31. T. Suzuki and T. F. Heinz, *Opt. Lett.* **124**, 1201 (1989).
32. X. D. Zhu, A. Lee, and A. Wong, *Appl. Phys.* **A52**, 317 (1991).

33. X. D. Zhu, Th. Rasing, and Y. R. Shen, *Chem. Phys. Lett.* **155**, 459 (1989).
34. X. D. Zhu, Y. R. Shen, and R. Carr, *Surf. Sci.* **163**, 114 (1985).
35. H. J. Eichler, P. Gunter, and D. W. Pohl, *Laser-Induced Dynamic Gratings* (Springer, 1986).
36. G. A. Somorjai, *Chemistry in Two Dimensions: Surfaces* (Cornell University Press, 1981).
37. J. H. Bechtel, *J. Appl. Phys.* **46**, 1585 (1975).
38. P. A. Redhead, *Vacuum* **123**, 203 (1962); D. A. King, *Surf. Sci.* **47**, 384 (1975).
39. X. D. Zhu, *Ph. D. thesis*, University of California, Berkeley, unpublished, (1989).
40. Y. R. Shen, *Ann. Rev. Phys. Chem.* **40**, 327 (1989).
41. J. D. McIntyre and D. E. Aspnes, *Surf. Sci.* **24**, 417 (1971).
42. A. Bagchi, R. G. Barrera, and A. K. Rajagopal, *Phys. Rev.* **B20**, 4824 (1979).
43. T. F. Heinz, C. K. Chen, D. Ricard, and Y. R. Shen, *Phys. Rev. Lett.* **46**, 1010 (1981).
44. Y. R. Shen, *The Principles of Nonlinear Optics* (Wiley, 1984), p. 494; *Ann. Rev. Mater. Sci.* **16**, 69 (1986).
45. P. Guyot-Sionnest and Y. R. Shen, *Phys. Rev.* **B33**, 8254 (1986).
46. Xudong Xiao, Yuanlin Xie, and Y. R. Shen, *Surf. Sci. Lett.* **271**, 295 (1992).
47. J. M. Blakely and M. Mykura, *Acta Metall.* **10**, 565 (1962).
48. H. P. Bonzel and E. E. Latta, *Surf. Sci.* **76**, 275 (1978).
49. P. S. Maiya and J. M. Blakely, *J. Appl. Phys.* **38**, 698 (1967).
50. K. Yamashita, H. P. Bonzel, and H. Ibach, *Appl. Phys.* **25**, 231 (1981).
51. S. M. George, A. M. DeSantolo, and R. B. Hall, *Surf. Sci.* **159**, L425 (1985).
52. D. A. Mullins, B. Roop, and J. M. White, *Chem. Phys. Lett.* **129**, 511 (1986).
53. S. Lehwald, J. M. Szeftel, H. Ibach, T. S. Rahman, and D. L. Mills, *Phys. Rev. Lett.* **50**, 518 (1983).
54. T. S. Rahman and H. Ibach, *Phys. Rev. Lett.* **54**, 1933 (1985); J. E. Mueller, M. Wuttig, and H. Ibach, *Phys. Rev. Lett.* **56**, 1583 (1986); M. Rocca, S. Lehwald, H. Ibach, T. S. Rahman, *Phys. Rev.* **B35**, 9510 (1987).
55. W. Daum, S. Lehwald, and H. Ibach, *Surf. Sci.* **178**, 528 (1986).
56. J. M. Szeftel, S. Lehwald, H. Ibach, T. S. Rahman, J. E. Black, and D. L. Mills, *Phys. Rev. Lett.* **51**, 268 (1983); T. S. Rahman, D. L. Mills, J. E. Black, J. M. Szeftel, S. Lehwald, and H. Ibach, *Phys. Rev.* **B30**, 589 (1984).
57. S. Lehwald, B. Voigtländer, and H. Ibach, *Phys. Rev.* **B36**, 2446 (1987); B. Voitgländer, S. Lehwald, and H. Ibach, *Surf. Sci.* **208**, 113 (1989).